European Polymer Journal 158 (2021) 110685

Contents lists available at ScienceDirect

European Polymer Journal

journal homepage: www.elsevier.com/locate/europolj

Molecular dynamics simulations of quinine encapsulation into biodegradable nanoparticles: A possible new strategy against Sars-CoV-2

Pierluigi Stipa [a], Stefania Marano [a], Roberta Galeazzi [b], Cristina Minnelli [b], Emiliano Laudadio [a,*]

[a] Department of Materials, Environmental Sciences and Urban Planning, Marche Polytechnic University, Ancona 60131, Italy
[b] Department of Life and Environmental Sciences, Marche Polytechnic University, Ancona 60131, Italy

ARTICLE INFO

Keywords:
Molecular dynamics
Biodegradable
SARS-CoV-2
PLA
PGA
PLGA

ABSTRACT

A new coronavirus disease, SARS-CoV-2, has spread into a global pandemic in December 2019. Since no specific therapeutic drugs for treating COVID-19 have been approved by FDA, recent studies suggest that the known antimalarial quinine and its derivatives (chloroquine and hydroxychloroquine) inhibit receptor binding of the viral particles and inhibits the strong "cytokine storm", which is the main cause of death among infected patients. In particular, the natural alkaloid quinine has shown to possess a better safety profile and greater tolerability compared to its derivatives. Dosage optimization of quinine is still necessary as the currently available dosage forms have controversial pharmacokinetics and safety profiles. Therefore, repurposing quinine dosage forms to improve its pharmacokinetics and safety profile may be necessary to support its use against SARS-CoV-2. In this context, biodegradable/biocompatible polymeric nanoparticles may provide a safe site-specific and controlled quinine delivery, reducing the frequency of drug administration and the dose.

In this study, a full atomistic molecular dynamics simulation approach has been used to investigate the use of poly-(glycolic acid) and poly-(lactic acid) and their copolymer poly-(lactic-co-glycolic acid) as potential delivery systems for lipophilic quinine to get insights into the mechanism of quinine encapsulation and release at the atomic/molecular level.

1. Introduction

In late December 2019 a new coronavirus was reported to cause a cluster of pneumonia cases in Wuhan, China [1,2]. On 11th February 2020 the International Committee on Taxonomy of Viruses named this novel coronavirus as severe acute respiratory syndrome coronavirus 2 (SARS-CoV-2), and the pneumonia was cataloged as coronavirus disease 2019 (COVID-19) by the World Health Organization (WHO) [3]. Due its high-transmissible characteristic, WHO announced COVID-19 as a global health emergency [4]. Since then, there has been continuous effort to develop therapeutic interventions against coronavirus infection, including the development of potentially effective vaccines from several manufactures as a reasonable prevention strategy to control the pandemic [5,6].

However, COVID-19 vaccine demand is sky-high and suppliers are struggling to provide the estimated 14 billion doses required by the end of 2021 [7]. Moreover, scientific, social, and political inquiries about doses, safety, schedule, ethics, effectiveness, surveillance, and vaccine hesitancy (global acceptability of vaccines varies from as low as 55% in Russia to as high as 90% in China) remain to be solved [8,9]. Therefore, in light of these issues and the current delays in vaccine implementation, the development of effective therapeutic treatments to support rapid recovery from COVID-9 is currently of outmost relevance.

In this context, small molecule-based therapies, which are approved for other diseases, are currently under investigations as they have shown to improve outcomes in COVID-19 patients diagnosed with severe pneumonia [10]. A particular research interest is giving to some antiviral drugs (chloroquine (CQ), hydroxychloroquine (HCQ), and quinine (QN)) which if administered shortly after symptoms' onset have shown to decrease infectiousness by reducing viral shedding in the respiratory secretions of COVID-19 patients [11–13]. These are well-known drugs, widely employed in the treatment and prophylaxis of malaria [14]. They all derived from quinoline alkaloid, a heterocyclic aromatic organic compound having a general molecular formula of C_9H_7N. However, the main difference lays to the fact that synthetically chloroquine/hydroxychloroquine belongs to the 4-aminoquinoline class, while the natural alkaloid quinine belongs to the 4-quinolinemethanol family [15,16].

Due to the structural similarities, they all are expected to act with a

* Corresponding author.
E-mail address: e.laudadio@staff.univpm.it (E. Laudadio).

https://doi.org/10.1016/j.eurpolymj.2021.110685
Received 27 May 2021; Received in revised form 29 July 2021; Accepted 2 August 2021
Available online 4 August 2021

similar mechanism of action against SARS-CoV-2, which could be mainly appointed to their capacity to interfere in various steps of the viral replication (i.e. by hindering viral entry to the cell and limiting viral-receptor interaction).

In this regard, current studies have mainly focused on the use of HCQ and CQ [17]. However, the interest in these drugs dramatically declined following the publication of a retrospective analysis claiming the occurrence of potential cardiac adverse effects after their administration in COVID-19 patients, which resulted in a rapid revocation of the FDA's emergency use authorization. Although this paper was soon after retracted due to data validity concerns, the use of HCQ and CQ remains controversial and further pharmacovigilance is still required [18,19].

On the other hand, the natural alkaloid QN is considered as a safer and well-tolerated medicine compared to CQ and HCQ [20]. In fact, besides its well-known antimalarial activity, QN is also used for the treatment of calf cramps [21], as well as for chronic autoimmune and rheumatic diseases [22]. Moreover, QN is widely added in beverages including tonic water and bitter lemon. Very recent *in vitro* and *in silico* works have shown that QN appears to exert a higher antiviral activity against SARS-CoV-2 with a significantly better toxicity profile if compared to the controversially discussed drugs HCQ and CQ [23,24].

However, severe oculotoxicity has been reported following unwanted overdose of QN [25], which could occur with the currently available dosage forms and routes of administration. QN comes in the form of soluble salts (i.e. hydrochloride, dihydrochloride, sulfate, bisulfate and gluconate are the most common) and it is typically given either orally or parentally [26]. The parental route of QN is complicated as hypotension may occur if the drug is given too rapidly, and venous thrombosis has been reported to occur occasionally following intravenous injections [27]. The oral absorption of QN salts from the gastrointestinal tract is very rapid, reaching peak concentrations within 1–3 h with bioavailability exceeding 75% [28]. However, high doses of QN are typically required due to its high tendency to bind with plasma proteins in healthy subjects, ranging from 69 to 92% [29]. This clearly concurs to increase the risk of side effects induced by QN.

Therefore, reformulation of QN to improve its pharmacokinetics and safety profile may be helpful to support its use to treat COVID-19 patients. Among all the available strategies, biodegradable/biocompatible polymeric nanoparticles (NP) may help to reduce QN side effects and improve its therapeutic efficiency by providing more site-specific and controlled drug delivery compared to conventional formulations [30,31]. In fact, a sustained release of the QN allows one to reduce the frequency of drug administration and the dose.

In this regard, Poly-(glycolic acid) (PGA) and poly-(lactic acid) (PLA) along with the copolymer poly-(lactic-co-glycolic acid) (PLGA) are the most popular among the various available FDA approved biodegradable polymers because of their long clinical history, good degradation characteristics and possibilities for controlled delivery of small molecules [32–34].

In this study, a full atomistic molecular dynamics (MD) simulation approach has been used to investigate the use of PLA, PGA, and PLGA polymers as potential drug delivery systems for lipophilic QN (logP = 3.44), with the final aim to gain knowledge of the mechanism of QN encapsulation and release at the atomic/molecular level. The polymers chosen have different degree of hydrophobicity, which could affect the drug partition into the polymer core. In turn, polymer hydrophobicity is crucial to stabilize highly lipophilic compounds within the polymer. However, a certain degree of drug freedom, achievable by lowering the polymer hydrophobicity, is also important to allow the drug to be properly released [35,36]. PLGA copolymer composed of lactic acid (hydrophobic) and glycolic acid (more hydrophilic) units in the ratio of 75/25 was chosen to investigate a system with an intermediate hydrophobic character when compared to pure PLA and PGA.

A particular attention was firstly paid to the behaviour of drug-free polymer NPs when in contact with physiological environment (i.e degree of compactness and hydration). The focus is then switched to the QN-loaded NP systems, whereby a detailed simulation on how the drug molecules behave (i.e. drug-drug and drug-polymer interactions) and diffuse within/from the polymer matrix is reported and discussed. Finally, NPs including curcumin (CM) were also simulated to compare our systems with those experimentally prepared. In fact, it is known that curcumin can be encapsulated and released in a controlled way from PLGA NPs [37]. Since the logP values and the molecular weights of QN and CM are very close, CM-polymer NPs were used as a control to validate the feasibility of QN-polymer NPs systems.

2. Materials and methods

The three-dimensional structures of QN (logP = 3.44) and CM (logP = 3.62) molecules were generated and conformational analysis were carried out in relation to vibrational frequencies and potential energy surfaces computed at the density functional theory (DFT) level using B3LYP/6-311G** [38,39]. Three polymer systems were modelled and built up with fully hydrated monomers using Material Science of MACROMODEL Maestro Schrodinger, suite following our previously validated protocol [40]. Briefly, the first system contained 112 Lactic Acid (LA) units in racemic forms (PLA), the second included 112 Glycolic Acid (GA) units (PGA), while the third was composed of 81 LA racemic units and 27 GA units to generate 75/25 (LA/GA) PLGA copolymer. To simulate the effects due to polydispersity, each polymer structure was repeated three times in the space with different chain lengths. The resulting PLA and PGA polymer systems totally contained 16 + 32 + 64 LA and GA chains respectively, while PLGA contained 12 + 23 + 46 LA and 4 + 8 + 15 GA units. The random composition of PLGA with 75% PLA and 25% PGA was chosen for this investigation. The specific number of units was modelled to generate polymeric systems at nanoscale level, in accordance with literature reports where polymer systems were approximately 30 nm in diameter, well-fitting within the accepted limits (20–100 nm) for drug delivery systems [41]. The accuracy in the reproduction of specific size system was due to the necessity to model the systems according to experimental preparations [42]. To simulate a physiological environment, each system was placed in a 16 nm^3 simulation box and solvated with 134,583 three-site transferrable intermolecular potential (TIP3P) water molecules [43] and 752 salt ions (376 Na^+ and 376 Cl^- explicit ions corresponding to a salt content of 0.15 M of NaCl). The systems were prepared in the presence and absence of QN molecules, for a total of six different systems: free PLA, free PGA, free PLGA, PLA-QN, PGA-QN, and PLGA-QN. Since the drug-loaded systems contained a total of 34 molecules of QN (MW = 324.4 g/mol) and 33 molecules of CM (MW = 368.38 g/mol), the number of drug molecules added were calculated in relation to the drug's molecular weight and the amount of water molecules to reproduce specific experimental conditions corresponding to 5 mg/ml of encapsulated drug, in line with other formulations [44]. Each QN molecule was randomly added in the core of the polymer structures to investigate the molecular drug motions along MD simulation.

All MD simulations have been performed using GROMACS 5.0.4 suite [45] and AMBER99SB force field [46] with specific parameter extensions to provide the accurate description of QN, CM molecules, and polymer chains. Systems have been minimized applying periodic box conditions in all directions, using a neighbor searching grid type; the cut-off distance for the short-range neighbor list was set to 1.4 nm. Electrostatic interactions have been included by implementing a fast smooth particle-mesh Ewald algorithm [47,48] with 1.4 nm distance for the Coulomb cut-off, which is considered the method of choice to obtain an accurate evaluation of long-range electrostatic interactions in large macromolecular systems [49,50].

Each system was subjected to two minimization steps using steepest descent and conjugate gradient algorithms and subsequent six preliminary equilibration steps based on 5 ns of annealing simulations to gradually reach the simulation temperature of 310 K and generate atomistic velocities. A weak temperature coupling (Berendsen

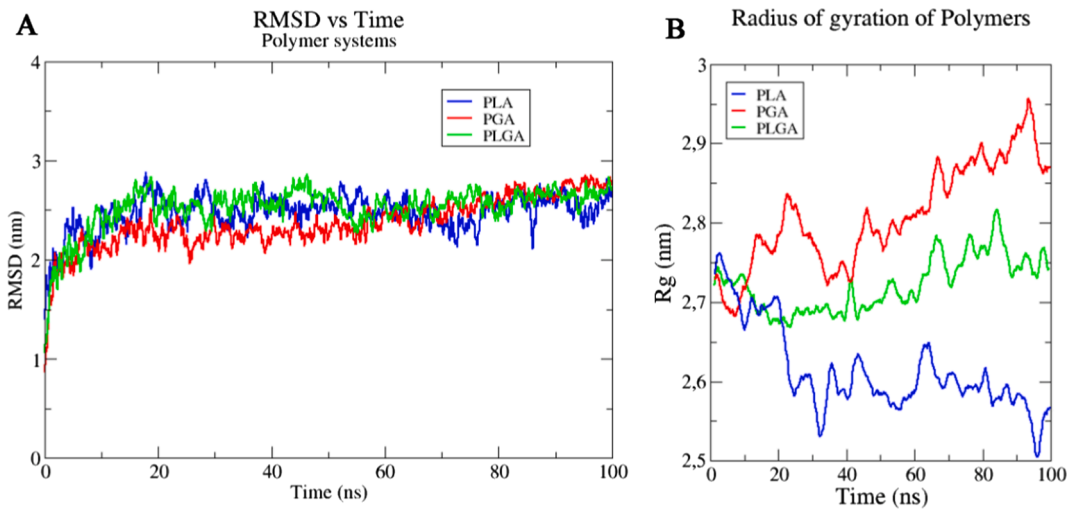

Fig. 1. (A) Root-Mean square deviation (RMSD) and (B) average radius of gyration of polymeric systems.

thermostat), with a time constant of 1 ps was applied to maintain the reference temperature (310 K) throughout the whole run. The subsequent production step consisted in 100 ns of MD simulation in isothermal – isobaric (NPT) ensemble at 1 atm and 310 K for each equilibrated system [51]. A time constant for coupling of 0.5 ps and an optimal compressibility for water of 4.5×10^{-5} bar^{-1} were used to obtain the best control of pressure. The achievement of a steady state for all of the simulated models was monitored through the molecular root-mean-square deviation (rmsd) values of polymer chains depending on simulation time [52]. Deviation was calculated in terms of displacement with respect to the starting minimized structure. The analysis of the simulations' trajectories was performed by means of VMD [53] and CHIMERA software [54]. The interactions of unloaded vectors with water were investigated to detect the polymers behavior (degree of compactness). Polymers' Surface Accessible Solvent Area (SASA) was calculated through the *gmx sasa* GROMACS tool to estimate the tendency of polymers to interact with water molecules, determining different hydration degrees, and the number of Hydrogen Bonds (HB) interactions were computed using the *gmx hbond* GROMACS tool. The compactness degree and convergence of simulations for polymers along MD simulation was determined by computing the radius of gyration (Rg) using *gmx gyrate* GROMACS tool. The potential energy interaction between QN and polymers was evaluated using the *gmx_energy* GROMACS tool, which takes into account both the polymer/drug hydrophobic and hydrophilic domains. The QN and CM release degrees were indirectly evaluated with radial distribution function (RDF) using the *gmx rdf* GROMACS tool. The reliability of these tools has been already demonstrated in previous studies [55,56].

3. Results and discussions

3.1. Pure polymer systems

To examine the adsorption of QN on the polymer surfaces and investigate the dynamic behavior of the drug molecules into the polymer systems, preliminary MD simulations were carried out on all polymeric systems under study before drug encapsulation. These systems were equilibrated and then analyzed in a physiological environment. Each polymeric vector was subjected to 100 ns of MD simulations in the presence of water molecules, as well as Na^+ and Cl^- ions. In order to evaluate the stability of the polymer systems, the root mean square deviation (rmsd) analysis were conducted, and the results are shown in Fig. 1A.

This analysis is necessary to assess whether the chosen simulation time is sufficient for the polymer systems to reach dynamic equilibrium. The extrapolated MD values show that deviation remained reasonably unchanged (i.e. did not exceed ~ 3 nm) till the end of the simulation time for all three polymeric models. Dynamic equilibrium was reached after 50 ns of simulation for each polymer, highlighting the high stability degree of the simulated systems.

To better verify the stability of the polymeric systems, the dynamic trajectories of polymeric structures were checked using radius of gyration (Rg) analysis (Fig. 1B). Starting from the same Rg values for all NPs at the beginning of MD simulations (i.e. about 2.7 nm), each polymer showed a specific behavior along MD simulation. Small Rg values indicate the polymer is relatively compact, meaning that the polymer adopts a folded structure throughout its trajectory. Focusing on the last 10 ns of MD simulations, PLA, PGA, and PLGA systems reached Rg values of 2.52 nm, 2.91 nm, and 2.74 nm respectively, maintaining these values with small fluctuations. This result confirms that the studied

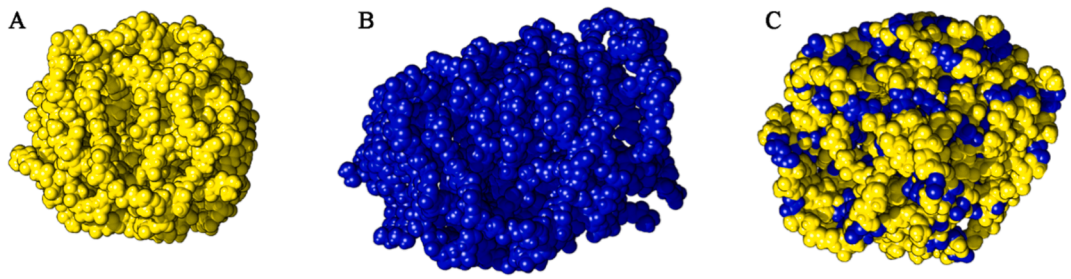

Fig. 2. Representative structures of PLA (A), PGA (B), and PLGA (C) at the end of 100 ns of MD simulation. The LA and the GA units are reported in yellow and blue Van der Waals spheres, respectively.

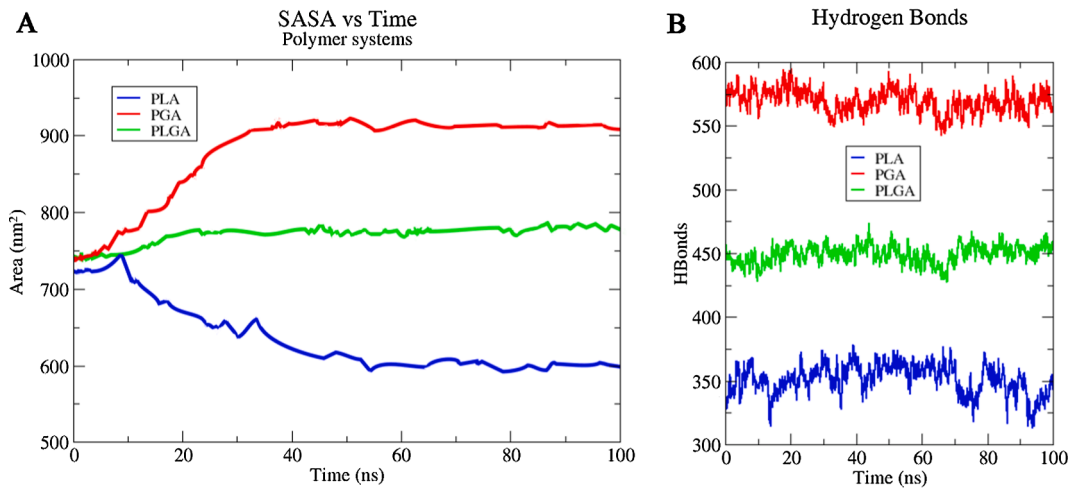

Fig. 3. Solvent accessible surface area (SASA) (A) and number of polymer-water hydrogen bonds (B).

systems are stable and behave differently in relation to the hydration properties of NPs.

The final snapshots of the investigated systems are displayed in Fig. 2.

Since the degree of compactness plays a critical role on the nanoparticle size, swelling, drug release rate, deformability, circulation time, stability, and agglomeration tendency, its investigation represents a very important feature for nanoparticulate system [57,58].

The MD results indicated that, as the monomer–monomer interactions became more attractive along 100 ns of simulations, polymeric chains could distinctly respond to confinement. More in details, PLA model showed the highest compactness degree along simulation (Fig. 2A), which accounts for its greater hydrophobic nature if compared to the other two polymeric systems, resulting in a more hydrophobically-stabilized structure. The absence of methyl side groups in PGA system leads to a very different behavior of the polymer vector, showing a marked tendency to interact with the solvent, which induced a visible polymer swelling (Fig. 2B). Concerning PLGA, its peculiar composition (25% PGA and 75% PLA), allows this copolymer to behave in a kind of intermediate way between pure PLA and PGA. It can be clearly seen that the predominance of PLA portion provides a discrete degree of compactness to the copolymer. On the other hand, the concomitant presence of more hydrophilic PGA regions maximized the interactions with both water through strong HB and Na^+ ions through ion–dipole interactions (Fig. 2C). This behavior typically results in higher rate of drug release when compared to pure PLA systems [59].

To better quantify the above reported polymers behavior in contact with the simulated physiological environment, the solvent accessible surface area (SASA) (Fig. 3A) and the number of HBs established b the polymer systems with water (Fig. 3B) have been calculated analyzing MD trajectories. Such methods are widely used to determine the degree of miscibility of polymeric systems once administered [60,61].

SASA values and HB number were obtained from the final part of the simulations (the last 10 ns) to ensure that a steady state was achieved. The calculated SASA average values and the number of HBs with water were about 608 nm^2 and 342 HBs for PLA, 918 nm^2 and 573 HBs for PLA 786 nm^2, and 476 HBs for PLGA. As expected, PLA displayed the lowest SASA value, which indicates a very low miscibility degree with the water phase. This behavior is related to the presence of the methyl groups in the PLA chain. This groups seems to play a fundamental role in favoring the interactions between the polymer chains, resulting in an overall lower affinity to the solvent compared to the other two systems. On the other hand, the PGA displayed the highest SASA value and HB number with the aqueous phase, confirming its greater tendency to interact with the water phase rather than with itself, likely due to the absence of

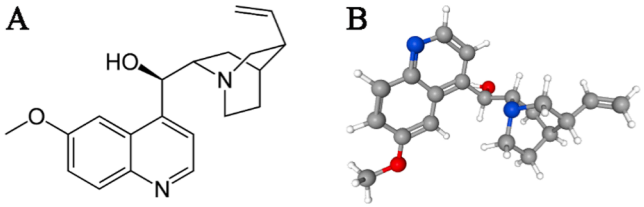

Fig. 4. 2D (A) and 3D (B) structure of quinine.

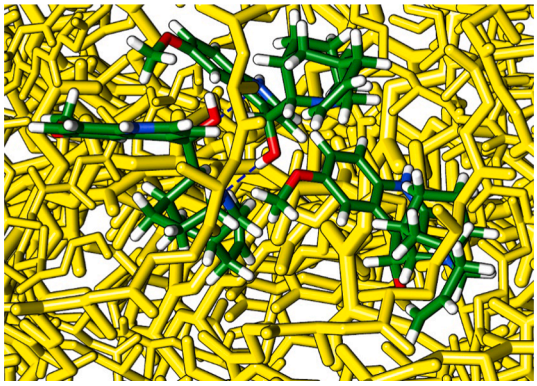

Fig. 5. PLA-QN model. The polymer chains are shown in yellow, while the C, O, N and H atoms of the quinine molecules are shown in green, red, blue, and white, respectively. The dashed blue lines indicate the HB between the QN molecules.

nonpolar methyl groups. This result confirmed that the drug molecules are not adequately protected, since polymers with larger SASA values are expected to undergo a faster hydrolysis. In the case of PLGA, the calculated SASA values and the number of polymer-water HB formation confirmed that this copolymer follows an intermediate behavior with respect to the other two systems, attributable to the presence of methyl groups in a lower extent with respect to pure PLA. Due to its discrete degree of compactness and affinity to the physiological environment, PLGA copolymer may be expected as the best candidate for QN drug delivery system when compared to the other two systems under investigation.

3.2. Polymer-quinine systems

The final structure obtained from the first MD simulation have been

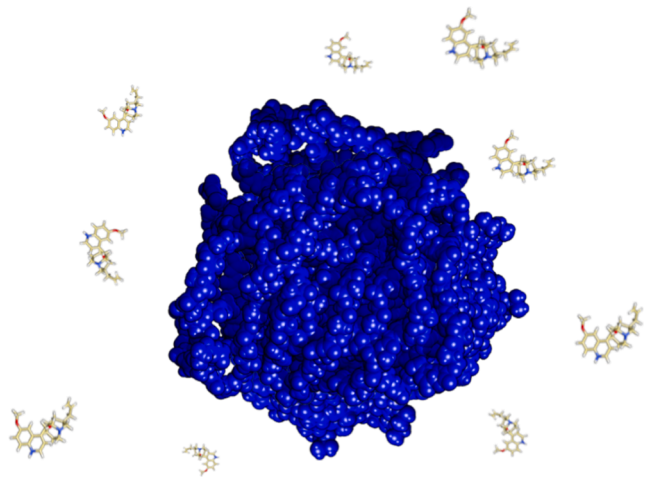

Fig. 6. PGA-QN model. The polymer chains are shown in blue spheres, while the C, O, N and H atoms of the quinine molecules are shown in yellow, red, blue and white, respectively. The red arrows emphasize the swelling tendency of the polymer system.

used as starting point to model polymer-drug systems. QN is a very lipophilic molecule but containing also some polar groups able to interact with polar moieties (Fig. 4 AB). The drug molecules were directly placed inside the polymers' cores, in order to simulate the experimental drug loading within the polymer systems.

The PLA polymer-based model was the first system investigated by means of the MD approach. During the simulation, the drug-polymer system proved to be extremely stable as drug molecules could strongly interact with hydrophobic LA monomer units. These interactions were observed for 100 ns following the same procedure for the drug-free PLA system. It can be observed that, due to the hydrophobic nature of both polymer and drug, QN molecules remained strongly aggregated inside the PLA core through QN-QN π-stacking and HB interactions (Fig. 5).

Stabilities and effectiveness of nanosuspensions can be influenced by polymer type, their molecular weight, and the kind of the encapsulated drug [62]. In the case of PLA-QN, the aggregation behavior is expected to have two main issues: the drug may not be properly released, and the formation of drugs' aggregates drastically decreases the drug bioavailability once released in a single step after polymer degradation.

Regarding PGA-QN model, MD simulations show that the addition of QN molecules into PGA core has a strong destabilizing effect on the whole system. More in details, at the very beginning of the simulation, it was observed that QN molecules look for a better conformational accommodation in the polymer core. This unambiguously indicates that

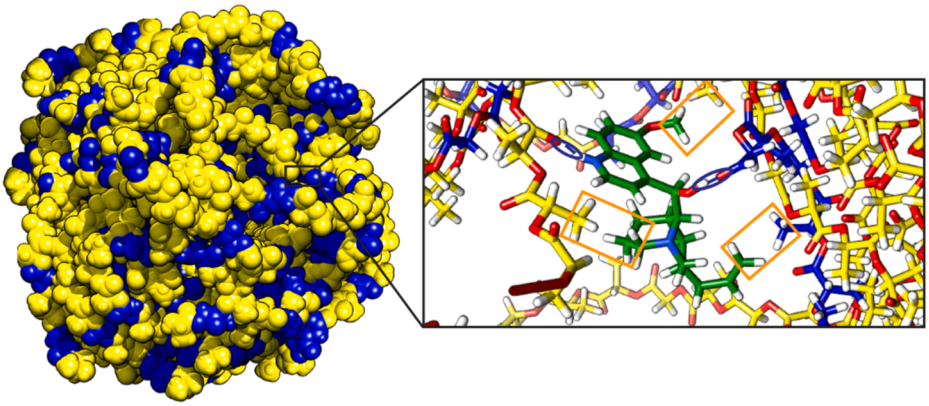

Fig. 7. PLGA-QN system. The polymer chains are shown in blue (glycolic acid) and yellow (lactic acid) spheres, while the C, O, N and H atoms of the quinine molecules are shown in green, red, blue, and white, respectively. The blue circles and the orange rectangles highlight respectively the hydrogen bonds and the nonpolar interactions observed between quinine and copolymer.

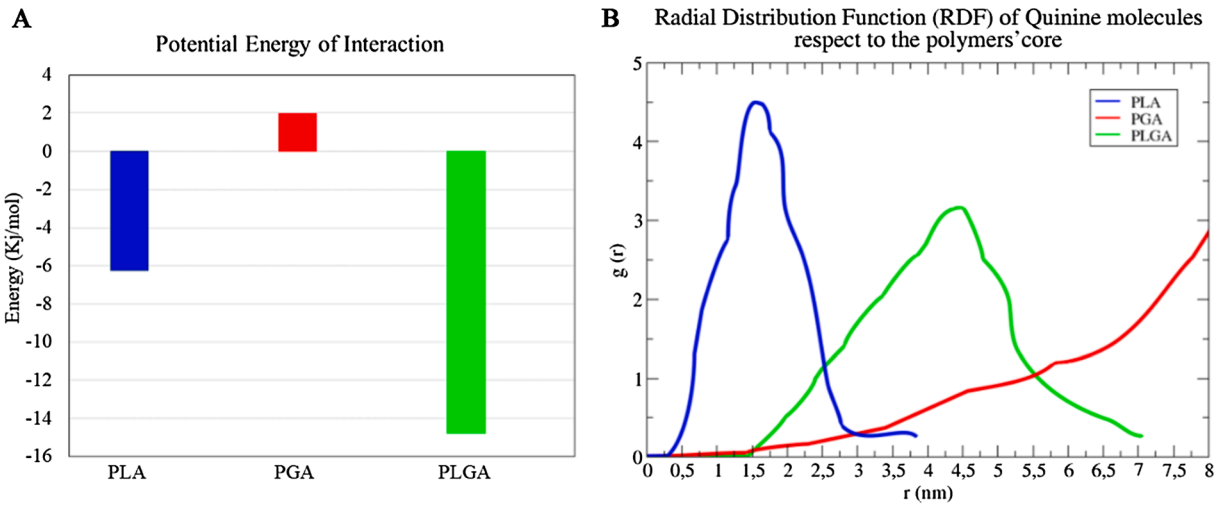

Fig. 8. Potential Energy Interaction between Quinine and Polymer systems (A) and Radial distribution function (RDF) (B) of the Quinine molecules respect to the polymers' cores in the investigated systems.

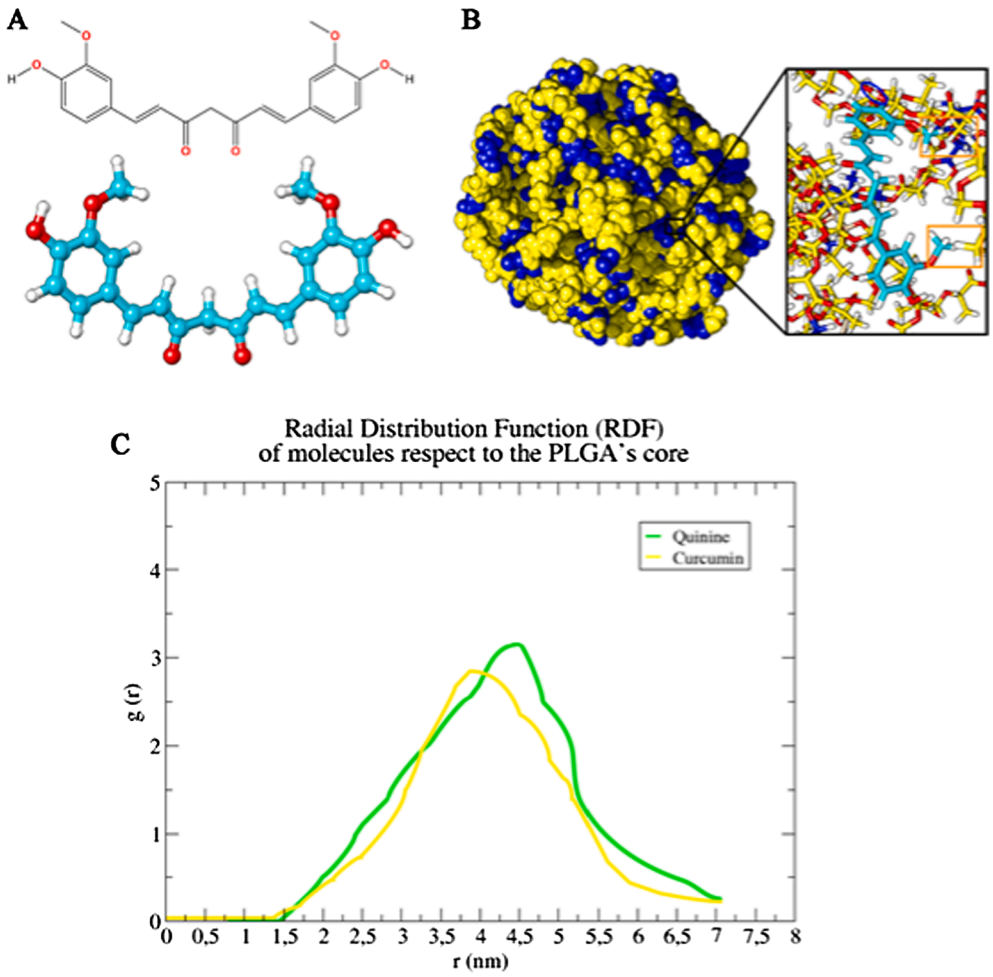

Fig. 9. (A) 2D and 3D structure of curcumin (CM) and (B)CM-PLGA system. The polymer chains are shown in blue (glycolic acid) and yellow (lactic acid) spheres, while the C, O, and H atoms of the CM molecules are shown in cyan, red, and white, respectively. The the orange rectangles highlight the nonpolar interactions observed between CM and copolymer. Radial distribution function (RDF) (C) of the QN and CM molecules respect to the PLGA's core.

the drug has no tendency to interact with PGA. This causes an increase in the free space in the polymer core as repulsive effects prevail between the chains, enhancing the interactions with the solvent, hence promoting the rapid diffusion of QN molecules from the polymeric core to the aqueous phase (Fig. 6). Similar behavior has been observed for other matrices of moderately hydrophilic polymers, in which the balance between dispersive and polar interactions leads to structure-morphological peculiarities, influencing the diffusion mechanism [63,64]. These observations strongly suggest that PGA is not appropriate for an effective QN delivery.

Finally, the PLGA-QN system model is based on the use of the copolymer formed by lactic acid and glycolic acid units, with a random order of succession that leads to the formation of an amorphous polymer. Analyzing MD trajectories during the 100 ns of simulation, such a system showed to be particularly stable, and it is possible to appreciate a homogeneous dispersion of QN molecules within the copolymer matrix promoted by strong polar (HBs) and nonpolar drug-polymer interactions (Fig. 7).

No drug-drug interactions were observed, and this is very important since any drug aggregates could have negative effects on the final drug bioavailability. No diffusion of QN to the aqueous phase was observed right after loading, meaning that drug-polymer interactions are able to stabilize the drug within the polymer.

To gain a deeper insight on the QN release from the polymer carriers, the potential energy interaction between drug molecules and polymers (Fig. 8A) and the QN radial distribution function (Fig. 8B) were computed. The data were obtained from the last 10 ns of MD simulations. The potential energy values are normalized in terms of kJ/mol per QN molecule. The values obtained between QN and PLA is negative (-6.18 kj/mol), because the drug molecules interact with the polymer core by nonpolar interactions. However, the drug-drug interactions avoid the optimal interactions with polymer vector. In contrast, positive values were found for the QN-PGA system (+1.68 kj/mol), because drug-polymer interactions are weak and the drug molecules preferentially interact with the water phase, and thus is quickly released. The QN-PLGA system showed the highest negative energy value (-14.72 kj/mol per QN molecule). This is because of drug molecules homogeneously diffused within the polymer matrix to establish site-specific nonpolar and HB drug-polymer interactions.

According to the Radial Distribution Function (RDF) shown in Fig. 8B, at a short distance it can be clearly seen that the RDF is zero. This is ascribed to strong repulsive forces between drug molecules when they are very close to each other (up to 0.3 nm). A sharp peak maximum appears at approximatively 1.45 nm for QN-PLA (in relation to the QN aggregates) and at 4.5 nm for QN-PLGA system (in relation to the homogeneous diffusion of the drug in the polymer matrix). No peaks were observed for QN-PGA system, because all drug molecules are quickly released interacting with the water phase.

These results confirm that the drug molecules are aggregated in the polymer core of PLA, while they are homogeneously distributed in the polymer when PLGA is used. It is necessary to mention that the obtained RDF peak intensity for Quinine-PLA system is related to the quinine-

quinine interactions that lead to a high presence of molecules at a specific distance from the polymer center. No defined RDF peaks are found for the Quinine-PGA system before a distance of 8 nm from the polymer center, for the reason, as previously discussed, the drug molecules tend to be quickly released in the water phase, moving away from the polymer cores.

In order to justify the feasibility of QN-PLGA system, a comparison with another PLGA-drug system was performed as a control. The small molecule of curcumin (CM) has been chosen (Fig. 9A), being its logP and molecular weight very similar to QN, and experimental studies about the encapsulation and the controlled release of CM in PLGA systems have been already performed [37]. The same approach adopted for QN-PLGA was used for CM-PLGA, allowing for a comparison to be made.

In details, after 100 ns of MD simulation, each CM molecule was surrounded by polymer chains (Fig. 9B), in a very similar way detected for PLGA-QN system. This means that no CM aggregates were found, key prerequisite for optimal drug release.

Comparing the RDFs of QN and CM molecules to the PLGA's core (Fig. 9C), sharp peaks appeared with maximum intensity at approximatively 4.5 nm for QN-PLGA system and 4 nm for CM-PLGA. This means that for both systems a homogeneous diffusion of the small molecules in the polymer matrix was found, with a little difference in values that could be ascribed to the slightly higher lipophilic character of CM (logP = 3.62) compared to QN (logP = 3.44).

4. Conclusions

Small molecule-based therapies have recently attracted a great deal of attention as a potential alternative strategy to fight the current global pandemic trigged by SARS-CoV-2. Among them, the administration of well-known antimalarial QN has shown promising results in terms of both efficiency and safety, if compared to the mostly studied QC and HQC parent compounds.

In this work, a full atomistic molecular dynamics simulation has been carried out to explore three different well-known biodegradable polymer systems (PLA, PGA, and PLGA 75/25) as potential candidates for the delivery of lipophilic QN. The results obtained showed that the three drug-unloaded polymer vectors have different tendency to interact with the simulated physiological environment, leading to different degree of compactness in the ascending order, PGA < PLGA < PLA.

More importantly, following QN incorporation, the analysis of the trajectories and the extrapolation of specific properties lead to the identification of the PLGA as the best-enslaved candidate. More in details, QN molecules remained strongly aggregated inside the PLA core through QN-QN π-stacking and HB interactions, which could detrimentally affect its release and bioavailability. In contrast, the observed weak QN-PGA interactions and the greater free volume found in PGA matrix promoted a fast diffusion of QN molecules to the water phase. On the other hand, in PLGA system, QN was found to be homogeneously distributed, establishing site-specific nonpolar and HB drug-polymer interactions. The similar behavior of QN-PLGA to CM-PLGA, which is a known PLGA-controlled release system, strongly suggests that PLGA matrix may be expected to provide a controlled QN release as a function of polymer erosion rate, which could promote a safer and effective therapeutic use of QN against SARS-CoV-2.

CRediT authorship contribution statement

Pierluigi Stipa: Conceptualization, Resources, Supervision. **Stefania Marano:** Investigation, Resources, Supervision. **Roberta Galeazzi:** Data curation, Validation. **Cristina Minnelli:** Conceptualization, Validation. **Emiliano Laudadio:** Data curation, Formal analysis, Investigation, Methodology, Project administration, Software, Supervision, Validation, Visualization, Writing–original draft, Writing–review & editing

Declaration of Competing Interest

The authors declare that they have no known competing financial interests or personal relationships that could have appeared to influence the work reported in this paper.

Acknowledgements

We would like to thank CINECA-HPC ISCRA MARCONI-100 computer system (project n. HP10CMPMGP).

References

[1] Q. Li, X. Guan, P. Wu, X. Wang, L. Zhou, Y. Tong, R. Ren, K.S.M. Leung, E.H.Y. Lau, J.Y. Wong, X. Xing, N. Xiang, Y. Wu, C. Li, Q.i. Chen, D. Li, T. Liu, J. Zhao, M. Liu, W. Tu, C. Chen, L. Jin, R. Yang, Q.i. Wang, S. Zhou, R. Wang, H. Liu, Y. Luo, Y. Liu, G.e. Shao, H. Li, Z. Tao, Y. Yang, Z. Deng, B. Liu, Z. Ma, Y. Zhang, G. Shi, T.T. Y. Lam, J.T. Wu, G.F. Gao, B.J. Cowling, B.o. Yang, G.M. Leung, Z. Feng, Early Transmission Dynamics in Wuhan, China, of Novel Coronavirus-Infected Pneumonia, N. Engl. J. Med. 382 (13) (2020) 1199–1207, https://doi.org/10.1056/NEJMoa2001316.

[2] N. Zhu, D. Zhang, W. Wang, X. Li, B. Yang, J. Song, X. Zhao, B. Huang, W. Shi, R. Lu, P. Niu, F. Zhan, X. Ma, D. Wang, W. Xu, G. Wu, G.F. Gao, W. Tan, A Novel Coronavirus from Patients with Pneumonia in China, N. Engl. J. Med. 382 (2020) (2019) 727–733, https://doi.org/10.1056/nejmoa2001017.

[3] A.E. Gorbalenya, S.C. Baker, R.S. Baric, R.J. de Groot, C. Drosten, A.A. Gulyaeva, B. L. Haagmans, C. Lauber, A.M. Leontovich, B.W. Neuman, D. Penzar, S. Perlman, L. L.M. Poon, D. Samborskiy, I.A. Sidorov, I. Sola, J. Ziebuhr, Severe acute respiratory syndrome-related coronavirus: The species and its viruses – a statement of the Coronavirus Study Group, BioRxiv (2020), https://doi.org/10.1101/2020.02.07.937862.

[4] World Health Organization (WHO), WHO Director-General's opening remarks at the mission briefing on COVID-19. [Online]. Available from: https://www.who.int/dg/ speeches/detail/who-director-general-s-opening-remarks-at-the-mission-briefing-on-covid-19 [Accessed on 1st March 2020], Https://Www.Who.Int/Dg/Speeches/Detail/Who-Director-General-S-Opening-Remarks-At-the-Media-Briefing-on-Covid-19—11-March-2020. (2020) 1. https://www.who.int/director-general/speeches/detail/who-director-general-s-opening-remarks-at-the-mission-briefing-on-covid-19—16-april-2020.

[5] C. Lee, W.J. Choi, Overview of COVID-19 inflammatory pathogenesis from the therapeutic perspective, Arch. Pharm. Res. 44 (1) (2021) 99–116, https://doi.org/10.1007/s12272-020-01301-7.

[6] Y. Li, R. Tenchov, J. Smoot, C. Liu, S. Watkins, Q. Zhou, A Comprehensive Review of the Global Efforts on COVID-19 Vaccine Development, ACS Cent. Sci. 7 (4) (2021) 512–533, https://doi.org/10.1021/acscentsci.1c00120.

[7] J.C. Castillo, A. Ahuja, S. Athey, A. Baker, E. Budish, T. Chipty, R. Glennerster, S. D. Kominers, M. Kremer, G. Larson, J. Lee, C. Prendergast, C.M. Snyder, A. Tabarrok, B.J. Tan, W. Więcek, Market design to accelerate COVID-19 vaccine supply, Science (80-) 371 (2021) 1107–1109, https://doi.org/10.1126/science.abg0889.

[8] M. Sallam, Covid-19 vaccine hesitancy worldwide: A concise systematic review of vaccine acceptance rates, Vaccines 9 (2021) 1–15, https://doi.org/10.3390/vaccines9020160.

[9] J.V. Lazarus, S.C. Ratzan, A. Palayew, L.O. Gostin, H.J. Larson, K. Rabin, S. Kimball, A. El-Mohandes, A global survey of potential acceptance of a COVID-19 vaccine, Nat. Med. 27 (2) (2021) 225–228, https://doi.org/10.1038/s41591-020-1124-9.

[10] A.A. Panoutsopoulos, Known drugs and small molecules in the battle for COVID-19 treatment, Genes Dis. 7 (4) (2020) 528–534, https://doi.org/10.1016/j.gendis.2020.06.007.

[11] M. Große, N. Ruetalo, M. Layer, D. Hu, R. Businger, S. Rheber, C. Setz, P. Rauch, J. Auth, M. Fröba, E. Brysch, M. Schindler, U. Schubert, Quinine inhibits infection of human cell lines with sars-cov-2, Viruses. 13 (4) (2021) 647, https://doi.org/10.3390/v13040647.

[12] B. Singh, H. Ryan, T. Kredo, M. Chaplin, T. Fletcher, Chloroquine or hydroxychloroquine for prevention and treatment of COVID-19, Cochrane Database Syst. Rev. 2020 (2020), https://doi.org/10.1002/14651858.CD013587.

[13] V.B. Pallaval, M. Kanithi, S. Meenakshisundaram, A. Jagadeesh, M. Alavala, T. Pillaiyar, M. Manickam, B. Chidipi, Chloroquine Analogs: An Overview of Natural and Synthetic Quinolines as Broad Spectrum Antiviral Agents, Curr. Pharm. Des. 27 (9) (2021) 1185–1193, https://doi.org/10.2174/1381612826666201211121721.

[14] C. Bianchini, Therapy and prophylaxis of malaria, Med. - Riv, Della Encicl. Medica Ital. 9 (1989) 27–40, https://doi.org/10.1001/jama.240.21.2293.

[15] A.K. Bhattacharjee, M.G. Kartell, D.A. Nichols, R.P. Hicks, J.E. Van Hamont, W.K. Milhous, In silico three dimensional pharmacophore models to aid the discovery and design of new antimalarial agents, in: Lect. Notes Comput. Sci. (Including Subser. Lect. Notes Artif. Intell. Lect. Notes Bioinformatics), 2006: pp. 387–394. https://doi.org/10.1007/11758501_54.

[16] A.K. Bhattacharjee, M.G. Hartell, D.A. Nichols, R.P. Hicks, B. Stanton, J.E. van Hamont, W.K. Milhous, Structure-activity relationship study of antimalarial indolo [2,1-b]quinazoline-6,12-diones (tryptanthrins). Three dimensional pharmacophore

modeling and identification of new antimalarial candidates, Eur. J. Med. Chem. 39 (1) (2004) 59–67, https://doi.org/10.1016/j.ejmech.2003.10.004.
[17] Y. Song, E. Fields, Pharmacological Advances of Chloroquine and Hydroxychloroquine: From Antimalarials to Investigative Therapies in COVID-19, Nat. Prod. Commun. 15 (2020), https://doi.org/10.1177/1934578X20953648.
[18] G. Cirino, A. Ahluwalia, The many mechanisms of action of Chloroquine: to use or not to use (in COVID-19) that is the question, Br. J. Pharmacol. 177 (15) (2020) 3361–3362, https://doi.org/10.1111/bph.v177.1510.1111/bph.15177.
[19] X. Li, Y. Wang, P. Agostinis, A. Rabson, G. Melino, E. Carafoli, Y. Shi, E. Sun, Is hydroxychloroquine beneficial for COVID-19 patients? Cell Death Dis. 11 (7) (2020) https://doi.org/10.1038/s41419-020-2721-8.
[20] A. Della Porta, K. Bornstein, A. Coye, T. Montrief, B. Long, M.A. Parris, Acute chloroquine and hydroxychloroquine toxicity: A review for emergency clinicians, Am. J. Emerg. Med. 38 (10) (2020) 2209–2217, https://doi.org/10.1016/j.ajem.2020.07.030.
[21] H.C. Diener, W. Baurecht, Tolerability, compliance, quality of life, and clinical outcome during treatment with quinine sulfate in patients with nocturnal calf cramps. A multicenter non-interventional study (NIS) in adults, MMW-Fortschritte Der Medizin. 161 (2019) 24–31, https://doi.org/10.1007/s15006-019-0921-x.
[22] R.I. Rynes, Antimalarial drugs in the treatment of rheumatological diseases, Br. J. Rheumatol. 36 (1997) 799–805, https://doi.org/10.1093/rheumatology/36.7.799.
[23] M. Große, N. Ruetalo, R. Businger, S. Rheber, C. Setz, P. Rauch, J. Auth, E. Brysch, M. Schindler, U. Schubert, Evidence That Quinine Exhibits Antiviral Activity against SARS-CoV-2 Infection In Vitro, Preprints 19 (2020). https://dialog.proquest.com/professional/docview/2420336477?accountid=15585%0Ahttps://whel-primo.hosted.exlibrisgroup.com/openurl/44WHELF_NHS/44WHELF_NHS_services_page?genre=preprint&atitle=Evidence+That+Quinine+Exhibits+Antiviral+Activity+against+SARS-Co.
[24] K. Lestari, T. Sitorus, S. Instiaty, J.L. Megantara, Molecular docking of quinine, chloroquine and hydroxychloroquine to angiotensin converting enzyme 2 (ACE2) receptor for discovering new potential COVID-19 antidote, J. Adv. Pharm, Educ. Res. 10 (2020) 1–4.
[25] A. Jaeger, Quinine and chloroquine, Medicine (Baltimore). 40 (3) (2012) 154–155, https://doi.org/10.1016/j.mpmed.2011.12.018.
[26] A.P. Hall, A.W. Czerwinski, E.C. Madonia, K.L. Evensen, Human plasma and urine quinine levels following tablets, capsules, and intravenous infusion, Clin. Pharmacol. Ther. 14 (1973) 580–585, https://doi.org/10.1002/cpt1973144part1580.
[27] K.F. Maxcy, Limitations to the Use of Quinine Intravenously in the Treatment of Malaria, Public Heal. Rep. 37 (1922) 693, https://doi.org/10.2307/4576329.
[28] S. Krishna, N.J. White, Pharmacokinetics of Quinine, Chloroquine and Amodiaquine: Clinical Implications, Clin. Pharmacokinet. 30 (4) (1996) 263–299, https://doi.org/10.2165/00003088-199630040-00002.
[29] G. Paintaud, G. Alvan, O. Ericsson, The reproducibility of quinine bioavailability, Br. J. Clin. Pharmacol. 35 (3) (1993) 305–307, https://doi.org/10.1111/j.1365-2125.1993.tb05698.x.
[30] M. Germain, F. Caputo, S. Metcalfe, G. Tosi, K. Spring, A.K.O. Åslund, A. Pottier, R. Schiffelers, A. Ceccaldi, R. Schmid, Delivering the power of nanomedicine to patients today, J. Control. Release. 326 (2020) 164–171, https://doi.org/10.1016/j.jconrel.2020.07.007.
[31] A.R. Bilia, V. Piazzini, C. Guccione, L. Risaliti, M. Asprea, G. Capecchi, M. C. Bergonzi, Improving on Nature: The Role of Nanomedicine in the Development of Clinical Natural Drugs, Planta Med. 83 (2017) 366–381, https://doi.org/10.1055/s-0043-102949.
[32] I. Bala, S. Hariharan, MNV.R. Kumar, PLGA nanoparticles in drug delivery: The state of the art, Crit. Rev. Ther. Drug Carrier Syst. 21 (5) (2004) 387–422, https://doi.org/10.1615/CritRevTherDrugCarrierSyst.v21.i510.1615/CritRevTherDrugCarrierSyst.v21.i5.20.
[33] J.H. Lee, Y. Yeo, Controlled drug release from pharmaceutical nanocarriers, Chem. Eng. Sci. 125 (2015) 75–84, https://doi.org/10.1016/j.ces.2014.08.046.
[34] Y. Ramot, M. Haim-Zada, A.J. Domb, A. Nyska, Biocompatibility and safety of PLA and its copolymers, Adv. Drug Deliv. Rev. 107 (2016) 153–162, https://doi.org/10.1016/j.addr.2016.03.012.
[35] J. Panyam, D. Williams, A. Dash, D. Leslie-Pelecky, V. Labhasetwar, Solid-state solubility influences encapsulation and release of hydrophobic drugs from PLGA/PLA nanoparticles, J. Pharm. Sci. 93 (7) (2004) 1804–1814, https://doi.org/10.1002/jps.20094.
[36] D.K. Sahana, G. Mittal, V. Bhardwaj, M.N.V.R. Kumar, PLGA nanoparticles for oral delivery of hydrophobic drugs: Influence of organic solvent on nanoparticle formation and release behavior in vitro and in vivo using estradiol as a model drug, J. Pharm. Sci. 97 (4) (2008) 1530–1542, https://doi.org/10.1002/jps.21158.
[37] L. Duse, M.R. Agel, S.R. Pinnapireddy, J. Schäfer, M.A. Selo, C. Ehrhardt, U. Bakowsky, Photodynamic therapy of ovarian carcinoma cells with curcumin-loaded biodegradable polymeric nanoparticles, Pharmaceutics 11 (6) (2019) 282, https://doi.org/10.3390/pharmaceutics11060282.
[38] P.J. Stephens, F.J. Devlin, C.F. Chabalowski, M.J. Frisch, Ab Initio calculation of vibrational absorption and circular dichroism spectra using density functional force fields, J. Phys. Chem. 98 (45) (1994) 11623–11627, https://doi.org/10.1021/j100096a001.
[39] A.D. Becke, Density-functional thermochemistry. III. The role of exact exchange, J. Chem. Phys. 98 (7) (1993) 5648–5652, https://doi.org/10.1063/1.464913.
[40] P. Stipa, S. Marano, R. Galeazzi, C. Minnelli, G. Mobbili, E. Laudadio, Prediction of drug-carrier interactions of PLA and PLGA drug-loaded nanoparticles by molecular dynamics simulations, Eur. Polym. J. 147 (2021) 110292, https://doi.org/10.1016/j.eurpolymj.2021.110292.
[41] E. Mahmoudinezhad, A. Marquardt, G. Eggeler, F. Varnik, Molecular dynamics simulations of entangled polymers: The effect of small molecules on the glass transition temperature, Procedia Comput. Sci. 108 (2017) 265–271, https://doi.org/10.1016/j.procs.2017.05.152.
[42] W.B. Liechty, D.R. Kryscio, B.V. Slaughter, N.A. Peppas, Polymers for drug delivery systems, Annu. Rev. Chem. Biomol. Eng. 1 (1) (2010) 149–173, https://doi.org/10.1146/annurev-chembioeng-073009-100847.
[43] P. Mark, L. Nilsson, Structure and dynamics of the TIP3P, SPC, and SPC/E water models at 298 K, J. Phys. Chem. A. 105 (43) (2001) 9954–9960, https://doi.org/10.1021/jp003020w.
[44] S. Qiu, J. Lai, M. Guo, K.e. Wang, X. Lai, U. Desai, N. Juma, M. Li, Role of polymers in solution and tablet-based carbamazepine cocrystal formulations, CrystEngComm. 18 (15) (2016) 2664–2678, https://doi.org/10.1039/C6CE00263C.
[45] M.J. Abraham, T. Murtola, R. Schulz, S. Páll, J.C. Smith, B. Hess, E. Lindah, Gromacs: High performance molecular simulations through multi-level parallelism from laptops to supercomputers, SoftwareX. 1–2 (2015) 19–25, https://doi.org/10.1016/j.softx.2015.06.001.
[46] J.R. Biller, H. Elajaili, V. Meyer, G.M. Rosen, S.S. Eaton, G.R. Eaton, The Amber biomolecular simulation programs, J. Magn. Reson. 236 (2013) 47–56.
[47] T. Darden, D. York, L. Pedersen, Particle mesh Ewald: An N·log(N) method for Ewald sums in large systems, J. Chem. Phys. 98 (12) (1993) 10089–10092, https://doi.org/10.1063/1.464397.
[48] R.W. Hockney, J.W. Eastwood, Computer Simulation Using Particles, 1988. https://doi.org/10.1887/0852743920.
[49] J.W. Eastwood, R.W. Hockney, D.N. Lawrence, P3M3DP-The three-dimensional periodic particle-particle/ particle-mesh program, Comput. Phys. Commun. 19 (2) (1980) 215–261, https://doi.org/10.1016/0010-4655(80)90052-1.
[50] C. Minnelli, E. Laudadio, G. Mobbili, R. Galeazzi, Conformational insight on WT- and mutated-EGFR receptor activation and inhibition by epigallocatechin-3-gallate: Over a rational basis for the design of selective non-small-cell lung anticancer agents, Int. J. Mol. Sci. 21 (2020) 1–17, https://doi.org/10.3390/ijms21051721.
[51] E. Laudadio, R. Galeazzi, G. Mobbili, C. Minnelli, A. Barbon, M. Bortolus, P. Stipa, Depth Distribution of Spin-Labeled Liponitroxides within Lipid Bilayers: A Combined EPR and Molecular Dynamics Approach, ACS Omega. 4 (3) (2019) 5029–5037, https://doi.org/10.1021/acsomega.8b0339510.1021/acsomega.8b03395.s001.
[52] R.D. Porasso, J.J. López Cascales, A criterion to identify the equilibration time in lipid bilayer simulations, Pap. Phys. 4 (0) (2012), https://doi.org/10.4279/pip.040005.
[53] R. Zhang, C. Gao, S. Pan, R. Shang, Fusion of GNSS and speedometer based on VMD and its application in bridge deformation monitoring, Sensors (Switzerland). 20 (3) (2020) 694, https://doi.org/10.3390/s20030694.
[54] E.F. Pettersen, T.D. Goddard, C.C. Huang, G.S. Couch, D.M. Greenblatt, E.C. Meng, T.E. Ferrin, UCSF Chimera - A visualization system for exploratory research and analysis, J. Comput. Chem. 25 (13) (2004) 1605–1612, https://doi.org/10.1002/(ISSN)1096-987X10.1002/jcc.v25:1310.1002/jcc.20084.
[55] Y. Deng, B. Roux, Computations of standard binding free energies with molecular dynamics simulations, J. Phys. Chem. B. 113 (8) (2009) 2234–2246, https://doi.org/10.1021/jp807701h.
[56] C. Minnelli, R. Galeazzi, E. Laudadio, A. Amici, D. Rusciano, T. Armeni, M. Cantarini, P. Stipa, G. Mobbili, Monoalkylated epigallocatechin-3-gallate (C18-EGCG) as novel lipophilic EGCG derivative: Characterization and antioxidant evaluation, Antioxidants 9 (3) (2020) 208, https://doi.org/10.3390/antiox9030208.
[57] A. Sahoo, R. Suryanarayanan, R.A. Siegel, Stabilization of Amorphous Drugs by Polymers: The Role of Overlap Concentration (C*), Mol. Pharm. 17 (11) (2020) 4401–4406, https://doi.org/10.1021/acs.molpharmaceut.0c00576.
[58] S. Saboo, U.S. Kestur, D.P. Flaherty, L.S. Taylor, Congruent Release of Drug and Polymer from Amorphous Solid Dispersions: Insights into the Role of Drug-Polymer Hydrogen Bonding, Surface Crystallization, and Glass Transition, Mol. Pharm. 17 (4) (2020) 1261–1275, https://doi.org/10.1021/acs.molpharmaceut.9b01272.
[59] S. Hurrell, R.E. Cameron, The effect of initial polymer morphology on the degradation and drug release from polyglycolide, Biomaterials. 23 (2002) 2401–2409, https://doi.org/10.1016/S0142-9612(01)00376-3.
[60] U.R. Dahal, Z. Wang, E.E. Dormidontova, Hydration and Mobility of Poly(ethylene oxide) Brushes, Macromolecules. 50 (17) (2017) 6722–6732, https://doi.org/10.1021/acs.macromol.7b01369.
[61] W.J. Dunn, M.G. Koehler, S. Grigoras, The Role of Solvent-Accessible Surface Area in Determining Partition Coefficients, J. Med. Chem. 30 (7) (1987) 1121–1126, https://doi.org/10.1021/jm00390a002.
[62] E. Bilgili, M. Rahman, D. Palacios, F. Arevalo, Impact of polymers on the aggregation of wet-milled itraconazole particles and their dissolution from spray-dried nanocomposites, Adv. Powder Technol. 29 (12) (2018) 2941–2956, https://doi.org/10.1016/j.apt.2018.09.039.
[63] A.L. Iordanskii, L.P. Razumovskii, A.V. Krivandin, T.L. Lebedeva, Diffusion and sorption of water in moderately hydrophilic polymers: From segmented polyetherurethanes to poly-3-hydroxybutyrate, Desalination. 104 (1-2) (1996) 27–35, https://doi.org/10.1016/0011-9164(96)00023-9.
[64] T. Ali, M.H. Shoaib, R.I. Yousuf, S. Jabeen, I.N. Muhammad, A. Tariq, Use of hydrophilic and hydrophobic polymers for the development of controlled release tizanidine matrix tablets, Brazilian J. Pharm. Sci. 50 (2014) 799–818, https://doi.org/10.1590/S1984-82502014000400016.